

An Accurate Edge-based FEM for Electromagnetic Analysis with Its Applications to Multiscale Structures

Yangfan Zhang¹, Pengfei Wang², Wenping Li² and Shunchuan Yang¹

¹School of Information and Electronic Engineering, Beihang University, Beijing, 100083, CN

²School of Physics, Beihang University, Beijing, 100083, CN

This paper introduces an accurate edge-based smoothed finite element method (ES-FEM) for electromagnetic analysis for both two-dimensional cylindrical and three dimensional cartesian systems, which shows much better performance in terms of accuracy and numerical stability for mesh distortion compared with the traditional FEM. Unlike the traditional FEM, the computational domain in ES-FEM is divided into nonoverlapping smoothing domains associated with each edge of elements, triangles in two dimensional domain and tetrahedrons in three dimensional domain. Then, the gradient smoothing technique is used to smooth the gradient components in the stiff matrix of the FEM. Numerical results show that the ES-FEM can obtain much more accurate results than the traditional FEM and is independent of distortion of background meshes, which shows great potential to solve practical electromagnetic problems.

Index Terms—Edge-based smoothing domain, finite element method, gradient smoothing technique, multiscale.

I. INTRODUCTION

The finite element method (FEM) is one of the most powerful numerical methods to solve practical engineering problems due to its strong capability of handling complex and multiscale structures [1] and inhomogeneous media [2]. In the computational electromagnetics (CEM), the FEM is widely used to solve various electromagnetic problems, like the electrostatic currents [3], magneticstatic problems [4], electromagnetic scattering [5], integrated circuits modeling [6], electrical-thermal co-simulations [7].

However, investigations found that the traditional FEM is quite sensitive to the quality of background meshes [1]. More specifically, equilateral triangles and regular tetrahedrons are much preferred to guarantee the accuracy. However, when complex or multiscale structures are discretized into many nonoverlapping elements, a large number of irregular elements may exist. Then, the accuracy of the FEM can be severely degenerated and even totally unacceptable. However, generation of high good quality triangles and tetrahedrons is quite challenging when multiscale and complex structures are involved [8]. Therefore, the results cannot be always trusted when the mesh quality cannot be guaranteed. In addition, when low order basis functions are used, only a low level of accuracy of results can be obtained. That implies that a large number of unknowns are required if we need accurate results [9].

In this paper, we address these two issues in the CEM by introducing the edge-based smoothed FEM (ES-FEM) to accurately solve the electrostatic problems in the two dimensional cylindrical system and three dimensional cartesian system. The ES-FEM was firstly introduced to solve non-electromagnetic problems by properly combining the traditional FEM and mesh-free methods, termed as smoothed point interpolation methods (S-PIMs) [10]. Various versions of smoothed FEM (SFEM) are proposed based on how to construct smoothing

domains, like node-based FEM (NS-FEM) [11], face-based FEM (FS-FEM) [12], edge-based FEM (ES-FEM) [13]. They all show better performance in terms of accuracy and numerical stability for thermal analysis [14], acoustic analysis [15] and computational mechanics [16]. In most of applications, the ES-FEM shows best performance among them. In [17], the FS-PIM is introduced for the electromagnetic analysis. It is found that the FS-PIM shows improved accuracy. We introduced the ES-FEM to model the high-speed interconnects [18] and the electrostatic lens [19]. In this paper, we introduced the ES-FEM for electromagnetic analysis and comprehensively investigate its numerical properties, which has significant performance improvement compared with the FEM.

This paper is organized as follows. In Section II, detailed formulations for the ES-FEM are presented. In Section III, its accuracy and numerical properties are comprehensively investigated through several numerical experiments. At last, we draw some conclusions in Section IV.

II. FORMULATIONS

A. Problem Configurations

There are various axis-symmetrical systems, like electrostatic lens [19], which can be simplified as two dimensional problems in cylindrical system. The boundary-value problems can be defined by the following partial differential equation (PDE) as

$$\frac{\partial^2 V}{\partial r^2} + \frac{1}{r} \frac{\partial V}{\partial r} + \frac{\partial^2 V}{\partial z^2} = f, \quad (1)$$

subject to the boundary condition

$$a \frac{\partial V}{\partial n} + \gamma V = q, \quad (2)$$

where V denotes the potential in the computational domain, f is the excitation, a and γ are constants for the third kind of boundary conditions which is the first kind of boundary condition with $a = 0$ and $\gamma \neq 0$, and the second kind of boundary condition with $a \neq 0$ and $\gamma = 0$.

For those fully three dimensional structures, the PDE for the three dimensional cartesian system can be defined as

$$-\frac{\partial}{\partial x} \left(\alpha_x \frac{\partial V}{\partial x} \right) - \frac{\partial}{\partial y} \left(\alpha_y \frac{\partial V}{\partial y} \right) - \frac{\partial}{\partial z} \left(\alpha_z \frac{\partial V}{\partial z} \right) + \beta V = f, \quad (3)$$

subject to the boundary condition

$$a \frac{\partial V}{\partial n} + \gamma V = q, \quad (4)$$

where $\alpha_x, \alpha_y, \alpha_z$ and β are constant material parameters, V denotes the potential, f is the excitation, a and γ are constants.

B. Formulations of the FEM

In the FEM, we formulate (1) and (3) into a set of linear equations with the expansion of V through linear basis functions in each element through the Ritz method [1]. In matrix form, those linear equations can be rewritten into

$$\mathbf{K}\phi - \mathbf{b} = \mathbf{0}, \quad (5)$$

where \mathbf{K} is assembled from its elemental entity K^e in cylindrical system given by

$$K^e = 2\pi \int_{\Omega} \nabla N^e \cdot (\nabla N^e)^T r dr dz. \quad (6)$$

In three dimensional cartesian system, K^e is expressed as

$$K^e = \int_{\Omega} \nabla N^e \cdot (\nabla N^e)^T d\Omega, \quad (7)$$

N^e is a linear shape function in the FEM.

C. Creation of Smoothing Domain

Assuming that the solution domain Ω has been divided into N_e nonoverlapping elements with N_n nodes and N_{eg} edges. For two dimensional domain, by connecting the centroid of each element with its neighbor nodes, as shown in Fig. 1(a), the smoothing domain Ω_k^s associated with the k th edge is created. Therefore, the whole computational domain Ω is divided into N_{eg} nonoverlapping smoothing domains. Each smoothing domain may consist of 3 or 4 segments and nodes depending on the location of the edge k .

For three dimensional domain, one of the sub-domain of the smoothing domain Ω_k^s for k th edge located in the i th tetrahedron is created by connecting the centroid of the tetrahedron element and two centroids of the triangle surfaces, which are shared by edge k and vertexes of edge k , as shown in Fig. 1(b). By assembling all sub-domains of k th edge, the k th smoothing domain is created.

In traditional FEM, each node has only interactions with those belonging to the same element. However, in the ES-FEM, each node interacts with those contributing to the same smoothing domain. That means the interactions are performed on the smoothing domain rather than triangle or tetrahedron elements, which makes the ES-FEM more accurate and more stable to irregular meshes, especially, for multiscale structures without increasing the overall count of unknowns compared with the traditional FEM.

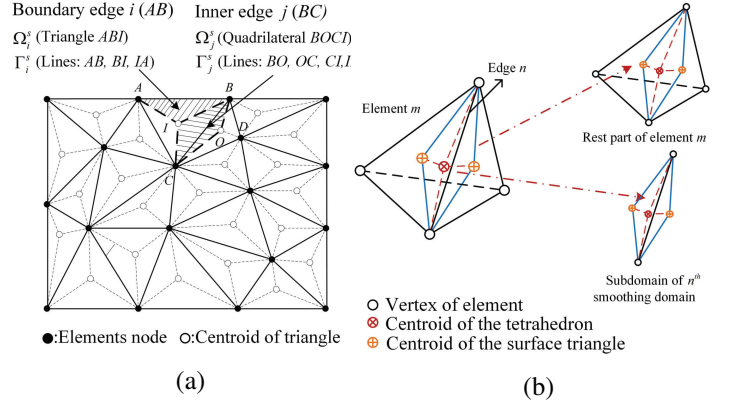


Fig. 1 Smoothing domains in (a) two and (b) three dimensional domain.

D. Detailed Formulations of the ES-FEM

The difference between the ES-FEM and the FEM lies in how we construct the stiff matrix which contains the gradient of the shape function ∇N . We first introduce the generalized gradient smoothing technique to replace the gradient component ∇N^e by its smoothed counterpart $\overline{\nabla N^e}$ [10]. In the ES-FEM formulation, the smoothed stiff matrix $\overline{K_d}$ can be expressed as

$$\overline{K_d} = \int_{\Omega} (\overline{\nabla N})^T \cdot \overline{\nabla N} d\Omega. \quad (8)$$

The generalized gradient smoothing technique [10] is applied in each smoothing domain by averaging the gradient shape function

$$\overline{\nabla N^e} = \int_{\Omega_k^s} \nabla N^e w(x - x_k) d\Omega, \quad (9)$$

where $w(x - x_k)$ denotes the smoothing function defined as

$$w(x - x_k) = \begin{cases} 1/\Delta_k & x \in \Omega_k^s \\ 0 & x \notin \Omega_k^s \end{cases}, \quad (10)$$

where Δ_k is area or volume of the k th smoothing domain in two or three dimensional domains, respectively. Through the divergence theorem, the gradient smoothed $\overline{\nabla N}$ can be expressed as

$$\begin{aligned} \overline{\nabla N^e} &= \int_{\Omega} \nabla N^e w(x - x_k) d\Omega \\ &= - \int_{\Omega} \nabla w(x - x_k) N^e d\Omega + \int_{\Gamma_k} \vec{n} N^e w(x - x_k) d\Gamma_k \\ &= \int_{\Gamma_k} \vec{n} N^e w(x - x_k) d\Gamma_k \end{aligned} \quad (11)$$

where Γ_k is the boundary of smoothing domain Ω_k^s , \vec{n} is the unit normal vector pointing to outside of the smoothing domain on Γ_k .

By substituting (11) into (9), it can be easy to be evaluated through Gaussian quadrature numerical integration as

$$(\overline{\nabla N})_d = \frac{1}{S_k} \int_{\Gamma_k} N n_d d\Gamma_k = \frac{1}{S_k} \sum_{i=1}^{N_b} w_i N(x_i) n_{id} l_i, \quad (12)$$

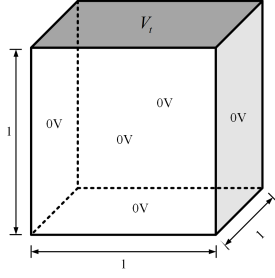


Fig. 2 Geometry configuration of the cubical box and boundary conditions.

where $d = r, z$ in two dimensional cylindrical domain and $d = x, y, z$ in three dimensional domain, N_b is the segment count of Γ_k , x_i and w_i are abscissas and weight for Gaussian numerical integration, respectively, n_{id} is the i th component of unit outward vector, l_i is the length of the i th segment. Therefore, we can denote the stiff matrix as

$$\overline{\nabla N(x_k)} = \sum_{j=1}^{n_k} \overline{B_j}(x_k) \quad (13)$$

where n_k is the number of nodes which contribute to the k th smoothing domain and \overline{B} is the smoothed gradient matrix which can expressed as

$$\overline{B_i}^T(x_k) = \frac{1}{S_k^s} \sum_{i=1}^{N_e^k} \frac{1}{3} S_e^i N_e^i \quad (14)$$

and

$$\overline{B_i}^T(x_k) = \frac{1}{S_k^s} \sum_{i=1}^{N_e^k} \frac{1}{6} S_e^i N_e^i \quad (15)$$

in two and three dimensional systems, respectively, N_e^k is the number of elements that share the edge k , Δ_e^i is the area or volume of the i th triangle or tetrahedron element.

By applying the boundary conditions and excitation exactly the same as those in the traditional FEM, we can solve the electromagnetic problems through the ES-FEM.

III. NUMERICAL RESULTS AND DISCUSSION

A. A Cubical Box

To analytically investigate the numerical properties of the ES-FEM, we first consider a cubical box as shown in Fig. 2. The top surface of cubical box is applied to a boundary condition

$$V_t = 10 \sin(\pi x) \sin(\pi y), \quad (16)$$

and other surfaces are set to 0 V. Therefore, the potential inside the box is given by

$$V_{ref} = \frac{10 \sin(\pi x) \sin(\pi y) \sinh(z\pi\sqrt{2})}{\sinh(\pi\sqrt{2})}. \quad (17)$$

Four background meshes with different mesh sizes are considered in our numerical analysis. In addition, to investigate the numerical stability of the ES-FEM, four irregular meshes, which are generated from a small random offset enforced at

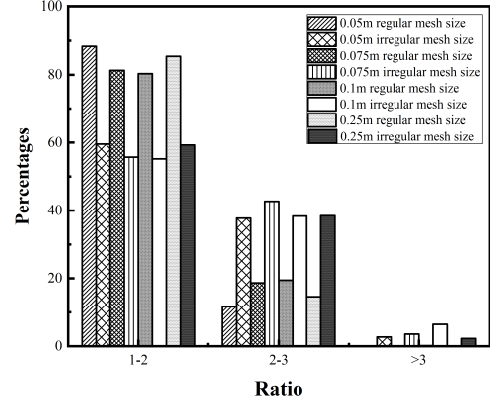


Fig. 3. Ratio distribution in four meshes.

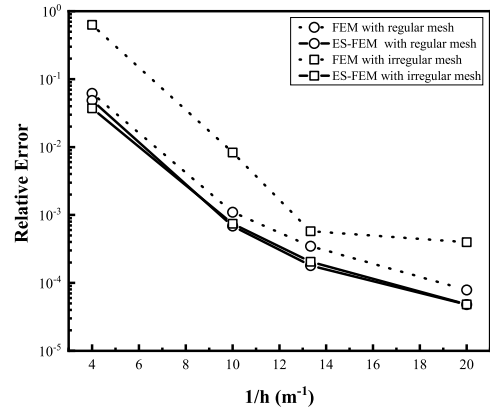


Fig. 4. Relative error obtained from the ES-FEM and the FEM with different meshes.

each node except boundary nodes in the regular meshes, are used. The averaged edge length of all elements is denoted as h . The relative error L_2 of V of all the nodes in the computational domain is defined as

$$L_2 = \sqrt{\frac{\sum_{i=1}^n (V_s^i - V_{ref}^i)^2}{\sum_{i=1}^n (V_{ref}^i)^2}}, \quad (18)$$

where V_s is the numerical result and V_{ref} is the reference potential obtained by (17).

Fig. 3 quantitatively illustrates the percentage of different ratio of elements in the four regular and irregular meshes used in the FEM and the ES-FEM. The ratio is defined as the maximum to minimum edge length in each element, which denotes mesh quality. Obviously, the ratio should be as near as one for good quality meshes. As shown in Fig. 3, the ratio of only around 20% of elements is larger than 2. However, in irregular meshes, the ratio of over 40% of elements is larger than 2, which implies that much more distorted elements exist in the irregular meshes.

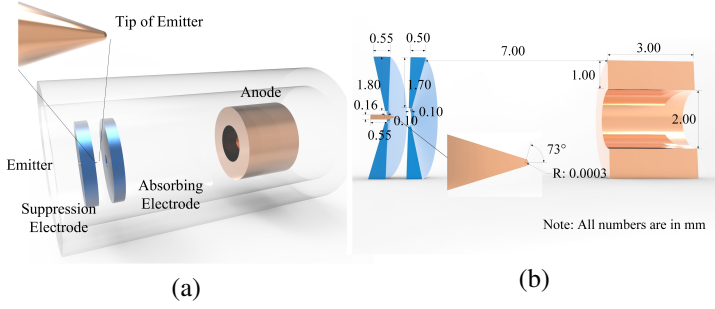


Fig. 5. Geometry configurations of the electronic lens.

Fig. 4 shows the relative error of the traditional FEM and the ES-FEM. It is easy to find that the ES-FEM outperforms the traditional FEM for both regular and irregular meshes. For regular meshes, the ES-FEM is more accurate than the FEM. When it comes to irregular meshes, it becomes more obvious. As shown in Fig. 4, the accuracy of the FEM is severely degenerated up to almost one order. However, the ES-FEM shows great numerical stability and its accuracy is not affected by the irregular meshes as shown in Fig. 4, which shows great numerical stability.

B. A Multiscale Electronic Lens

A multiscale electronic lens is considered which consists of an emitter, a suppression electrode, an absorbing electrode and an anode, as is shown in Fig. 5(a). Detailed geometry configurations are demonstrated in Fig. 5(b). The size of the whole structure is 12 millimeters, but the size of the emitter tip is only 0.0003 millimeters. The ratio of the size of the electronic lens to the size of the emitter tip reaches 10^5 , which is a typical multiscale structure.

As we can see, an electronic lens is an axis-symmetric structure which can be simplified into a two dimensional model. The potential of the emitter, the absorbing electrode and the anodes are set to 0 V, 7,000 V and 70,000 V, respectively. Both the cylindrical ES-FEM and fully three dimensional ES-FEM are applied in this case. Since the potential at the axis is quite important for the design, we extract the potential at the central axis to verify the accuracy of FEM and ES-FEM.

Fig. 6 shows that the ratio of elements in the four meshes used in our simulations. As shown in Fig. 6, the ratio of almost 40% elements is larger than 2. Further investigations find most irregular elements exist near the tip of the emitter. Since the lens is a multiscale structure, the quality of meshes cannot be improved no matter how we refine the meshes. As we mentioned in the introduction section, it is challenging to generate good quality meshes for multiscale structures. Since the FEM is sensitive to mesh quality, the accuracy cannot be guaranteed for multiscale structures.

The whole solution domain is first divided into 290,953 nonoverlapping tetrahedrons with 64,765 nodes and 387,700 edges. The overall count of unknowns in the FEM and the ES-FEM are 64,765. The potential along the central axis obtained from the ES-FEM with the linear shape function, the traditional FEM with the linear shape function. The reference

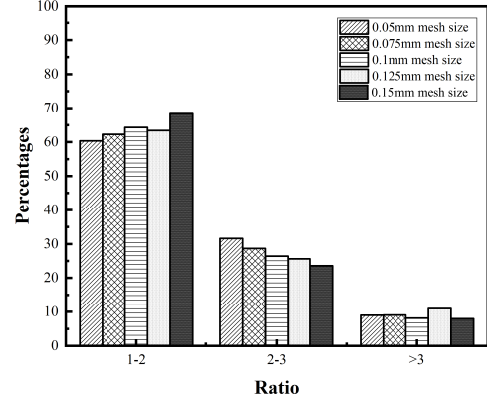


Fig. 6. Ratio distribution in four meshes.

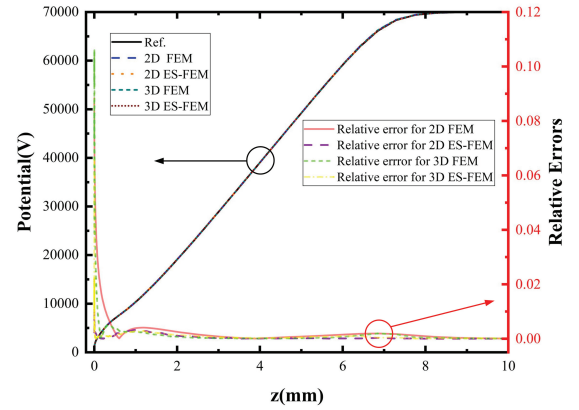


Fig. 7. Potential and relative errors of the electronic lens along the axis.

solution is obtained from the Comsol with 278,488 unknowns and the curved second order shape function.

Potential and relative errors along the axis are shown in Fig. 7. Both the 2D and 3D ES-FEM can obtain much more accurate results, especially in the mesh distortion region, near the tip of the emitter, compared with the FEM. The relative errors of the traditional FEM reach 2%, which is almost 20 times of that of the ES-FEM results. The ES-FEM can nearly immune to the distortion mesh due to the smoothing gradient technique. Furthermore, numerical results show that the ES-FEM in two dimensional system performs better than its three dimensional counterpart due to the geometry symmetry which reduces the error caused by mesh discretization in multiscale structures. The relative errors of the 3D ES-FEM with 4 different meshes is shown in Fig. 8. It is easy to find that the ES-FEM is much more accurate than the traditional FEM.

C. A Micromotor

We consider a electrostatic micromotor, which is a fully three dimensional structure [20]. Due to its symmetrical property, only a quarter of the structure is considered, which has

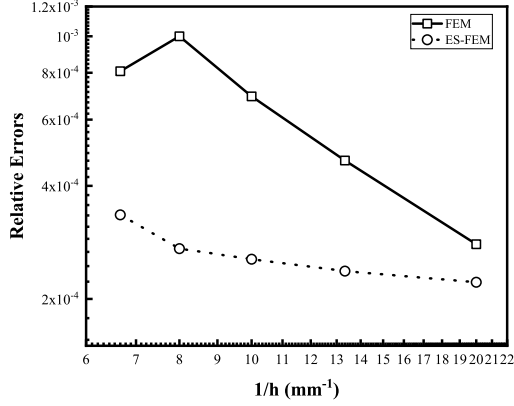


Fig. 8. Relative error of the electronic lens with four different meshes.

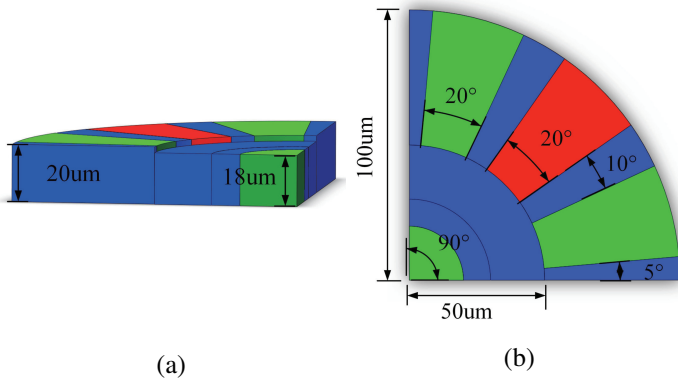


Fig. 9. Geometry configurations of the micromotor.

3 poles at stator and 2 poles at the rotor. The radius of stator is $100\text{ }\mu\text{m}$ with $20\text{ }\mu\text{m}$ in height. The inner and outer radius of the rotor are $20\text{ }\mu\text{m}$ and $50\text{ }\mu\text{m}$ with $18\text{ }\mu\text{m}$ in height, respectively. The potential of the central stator tooth is set to 100 V and other teeth are set to 0 V . Other boundaries are set as Neumann boundary conditions.

The whole solution domain is first discretized into 45,519 nonoverlapping tetrahedrons with 8,839 nodes and 56,815 edges. The potential distribution is computed at $z = 12\text{ }\mu\text{m}$ plane as shown in Fig. 10. The potential is also evaluated at $r = 49\text{ }\mu\text{m}$ in the $z = 12\text{ }\mu\text{m}$ plane. The reference solution is the numerical solution computed by the FEM with a fine mesh with 509,451 unknowns. As shown in Fig. 10, the ES-FEM with much less unknowns can obtain the exactly the same pattern as the reference. Furthermore, as shown in Fig. 11, the potential obtained from the ES-FEM agree well with the reference solution. It implies that the ES-FEM can solve complex electromagnetic structures.

IV. CONCLUSION

In this paper, we introduce the ES-FEM to accurately solve two dimensional cylindrical and three dimensional electromagnetic problems. By applying the generalized gradient

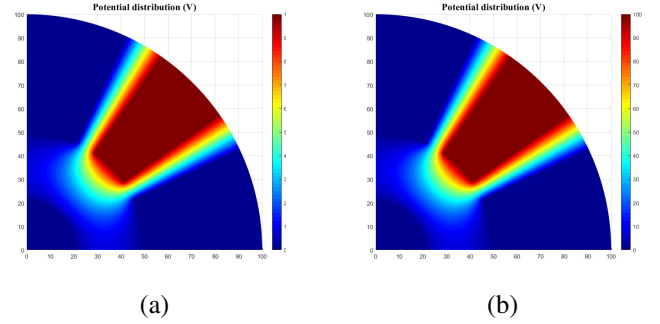


Fig. 10. Potential distribution of the micromotor obtained with (a) the FEM with a very fine mesh and (b) the ES-FEM with a coarse mesh.

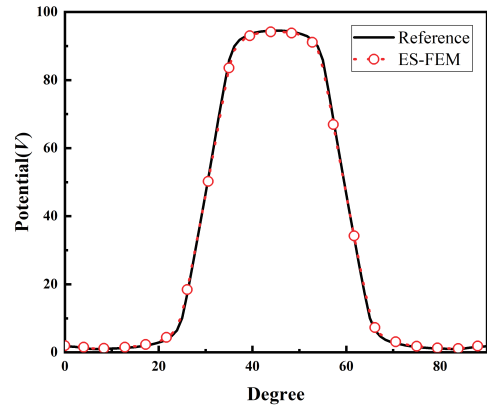


Fig. 11. Potential at $z = 12\text{ }\mu\text{m}$, $r = 49\text{ }\mu\text{m}$ obtained from the FEM with a very fine mesh and the ES-FEM with a coarse mesh.

smoothing technique to smoothing the gradient component in the FEM and constructing the smoothing domains based on all edges in the background meshes, a highly accurate and numerically stable ES-FEM is constructed. As numerical results show, the ES-FEM can indeed obtain much more accurate results and is stable to irregular meshes, especially when a large number of irregular meshes may exist in the multiscale structures. Therefore, it shows great potential to solve practical electromagnetic problems.

ACKNOWLEDGMENT

The authors would like to thank financial supports from Beijing Natural Science Foundation through Grant 4194082, National Natural Science Foundation of China through Grant 61801010, and Fundamental Research Funds for the Central Universities.

REFERENCES

- [1] J. M. Jin, *The finite element method in electromagnetics*. John Wiley&Sons, 2014.
- [2] S. H. Lee, K. Mao, and J. M. Jin, "A Complete Finite-Element Analysis of Multilayer Anisotropic Transmission Lines From DC to Terahertz Frequencies," *IEEE Trans. Adv. Packag.*, vol. 31, pp. 326-338, Jun. 2008.

- [3] T. Wang, R. F. Harrington, and J. R. Mautz, "Quasistatic analysis of a microstrip via through a hole in a ground plane," *IEEE Trans. Microw. Theory Tech.*, vol. 36, no. 6, pp. 1008-1013, 1988.
- [4] P. P. Silvester and R. L. Ferrari, *Finite Elements for Electrical Engineers*. 2nd ed., Cambridge: Cambridge University Press, 1990.
- [5] A. F. Peterson and S. P. Castillo, "A frequency-domain differential equation formulation for electromagnetic scattering from inhomogeneous cylinders," *IEEE Trans. Antennas Propagat.*, vol. 37, pp. 601607, Jun. 1989.
- [6] S. H. Lee, K. Mao, and J. M. Jin, "A complete finite-element analysis of multilayer anisotropic transmission lines from DC to terahertz frequencies," *IEEE Trans. Adv. Packag.*, vol. 31, pp. 326338, Jun. 2008.
- [7] T. Lu, J. M. Jin, "Electrical-Thermal Co-Simulation for Analysis of High-Power RF/Microwave Components," *IEEE Trans. Electromagn. Compat.*, vol. 59, no. 1, pp. 93-102, Sep. 2016.
- [8] G. Liu, *Meshfree methods: moving beyond the finite element method*. 2nd edn. CRC Press, 2009.
- [9] G. Liu, H. Nguyen-Xuan, and T. Nguyen-Thoi, "A theoretical study on the smoothed FEM (S-FEM) models: Properties, accuracy and convergence rates," *Int. J. Numer. Meth. Engng*, vol. 84, pp. 1222-1256, Dec. 2010.
- [10] G. Liu, N. Trung, *Smoothed finite element methods*. CRC press, 2016.
- [11] G. Liu, T. Nguyen-Thoi, and H. Nguyen-Xuan, "A node-based smoothed finite element method (NS-FEM) for upper bound solutions to solid mechanics problems," *Comput. Meth. Appl. Mech. Eng.*, vol. 87, no. 2, pp. 14-26, Jan. 2009.
- [12] T. Nguyen-Thoi, G. Liu, and K. Lam, "A facebased smoothed finite element method (FS-FEM) for 3D linear and geometrically non-linear solid mechanics problems using 4-node tetrahedral elements," *Int. J. Numer. Methods Eng.*, vol. 78, no. 3, pp. 324353, Apr. 2009.
- [13] Z. He, G. Liu, and Z. Zhong, "An edge-based smoothed finite element method (ES-FEM) for analyzing three-dimensional acoustic problems," *Comput. Meth. Appl. Mech. Eng.*, vol. 199, pp. 2033, Dec. 2009.
- [14] E. Li, G. Liu, "Simulation of hyperthermia treatment using the edge-based smoothed finite-element method," *Numer. Heat Transf. A-Appl.*, vol. 57(11), pp. 822847, Jun. 2010.
- [15] Z. He, A. Cheng, and Z. Zhong, "Dispersion error reduction for acoustic problems using the edge-based smoothed finite element method (ESFEM)" *Int. J. Numer. Methods Eng.*, vol. 86, no. 11, pp. 13221338, Jun. 2011.
- [16] T. Nguyen-Thoi, G. Liu, and H. Nguyen-Xuan, "Additional properties of the node-based smoothed finite element method (NS-FEM) for solid mechanics problems," *Int. J. Numer. Methods Eng.*, vol. 6, no. 4, pp. 633-666, 2009.
- [17] Lima, Nasses Z., and Renato C. Mesquita, "Face-based gradient smoothing point interpolation method applied to 3-D electromagnetics," *IEEE Trans. Magn.*, vol. 50, no. 2, pp. 537-540, Feb. 2014.
- [18] Y. Zhang, S. Yang, and D. Su, "An Edge-based Smoothed FEM for Accurate High-Speed Interconnect Modeling," in Conf. Numerical Electromagnetic and Multiphysics Modeling and Optimization, Boston, U.S.A., May. 2019.
- [19] Y. Zhang, P. Wang, W. Li and S. Yang, "An Edge-Based Smoothed FEM for Multiscale Electrostatic Lens Modeling," in Conf. ICEAA-IEEE APWC, Granada, Spain, Sep. 2019.
- [20] F. Guimaraes, R. Saldanha, R. Mesquita, D. Lowther, and J. Ramirez, "A meshless method for electromagnetic field computation based on the multiquadric technique", *IEEE Trans. Magn.*, vol. 43, no. 4, pp. 12811284, May. 2007.